frontiers | Frontiers in Chemistry

TYPE Original Research
PUBLISHED 09 November 2023
DOI 10.3389/fchem.2023.1279355

OPEN ACCESS

EDITED BY
Shamsa Bibi,
University of Agriculture, Faisalabad, Pakistan

REVIEWED BY
Anex Jose,
Stanford University, United States
Muhammad Abdul Qayyum,
University of Education Lahore, Pakistan

*CORRESPONDENCE
Aftab Hussain,
aftab.chem@pu.edu.pk
Farah Kanwal,
farahkchem@yahoo.com

RECEIVED 17 August 2023
ACCEPTED 20 October 2023
PUBLISHED 09 November 2023

CITATION
Hussain A, Irfan A, Kanwal F, Afzal M, Chaudhry AR, Hussien M and Ali MA (2023), Exploration of violet-to-blue thermally activated delayed fluorescence emitters based on "CH/N" and "H/CN" substitutions at diphenylsulphone acceptor. A DFT study.
Front. Chem. 11:1279355.
doi: 10.3389/fchem.2023.1279355

Exploration of violet-to-blue thermally activated delayed fluorescence emitters based on "CH/N" and "H/CN" substitutions at diphenylsulphone acceptor. A DFT study

Aftab Hussain[1]*, Ahmad Irfan[2], Farah Kanwal[1]*, Muhammad Afzal[1], Aijaz Rasool Chaudhry[3], Mohamed Hussien[2] and Muhammad Arif Ali[4]

[1]School of Chemistry, University of the Punjab, Lahore, Pakistan, [2]Department of Chemistry, College of Science, King Khalid University, Abha, Saudi Arabia, [3]Department of Physics, College of Science, University of Bisha, Bisha, Saudi Arabia, [4]Institute of Chemistry, Baghdad Campus, The Islamia University of Bahawalpur, Bahawalpur, Pakistan

The violet-to-blue thermally activated delayed fluorescence (TADF) emitters were created employing several substituents based on 5,5-dimethyl-5,10-dihydropyrido [2,3-b][1,8] naphthyridine-diphenylsulphone (**DMDHPN-DPS**) called **1a** via "CH/N" and "H/CN" substitutions at the diphenylsulphone acceptor (**DPS**) moiety. The parent compound **1a** was selected from our former work after extensive research employing "CH/N" substitution on Dimethyl-acridine (**DMAC**) donor moiety. There is a little overlap amid the highest occupied molecular orbitals (HOMOs) and lowest un-occupied molecular orbitals (LUMOs) due to the distribution of HOMOs and LUMOs primarily on the **DMDHPN** donor and the **DPS** acceptor moieties, respectively. It resulted in a narrower energy gap (ΔE_{ST}) between the lowest singlet (S_1) and triplet (T_1) excited state. In nearly all derivatives, the steric hindrance results in a larger torsional angle (85°–98°) between the plane of the **DMDHPN** and the **DPS** moieties. The predicted ΔE_{ST} values of the compounds with "H/CN" substitution were lower than those of the comparable "CH/N" substituents, demonstrating the superiority of the reversible inter-system crossing (RISC) from the $T_1 \rightarrow S_1$ state. All derivatives have emission wavelengths (λ_{em}) in the range of 357–449 nm. The LUMO → HOMO transition energies in the S_1 states are lowered by the presence of –CN groups or –N = atoms at the ortho or meta sites of a **DPS** acceptor unit, causing the λ_{em} values to red-shift. Furthermore, the λ_{em} showed a greater red-shift as there were more–CN groups or –N = atoms. Three of the derivatives named **1b**, **1g**, and **1h**, emit violet (394 nm, 399 nm, and 398 nm, respectively), while two others, **1f** and **1i**, emit blue shade (449 nm each) with reasonable emission intensity peak demonstrating that these derivatives are effective violet-to-blue TADF nominees. The lower ΔE_{ST} value for derivative **1i** (0.01 eV) with λ_{em} values

of 449 nm make this molecule the finest choice for blue TADF emitter amongst all the studied derivatives. We believe our research might lead to the development of more proficient blue TADF-OLEDs in the future.

KEYWORDS

diphenylsulphone (DPS), thermally activated delayed fluorescence (TADF), singlet-triplet energy gap (ΔE_{ST}), organic light emitting diode (OLED), reverse intersystem crossing (RISC), DFT, TD-DFT, HOMO-LUMO

1 Introduction

Owing to their potential use as solid-state lightening sources and high-resolution flat panel display, organic light-emitting diodes (OLEDs) having multi-layer structures got a lot of interest since Tang and his colleagues initially described them (Tang and VanSlyke, 1987; Adachi et al., 2001; Zhang et al., 2014a; Chan et al., 2018; Liu et al., 2018; Wada et al., 2020). Because traditional fluorescent material can only harvest singlet excitons, OLEDs can only attain an internal quantum efficiency (IQE) of 25% (Shuai et al., 2000; Mehes et al., 2012; Sun et al., 2015). In contrast, noble heavy-metal-based phosphorescent materials may harvest both singlets as well as triplet excitons and hence can achieve an IQE of ≈ 100% through effective spin-orbit coupling interaction (SOC) (Adachi et al., 2001; Deaton et al., 2010; Zhang et al., 2012a; Xu et al., 2021). Noble metal-containing phosphorescent materials are, however, rather expensive and unreliable for blue emission. Therefore, a novel approach for obtaining high photoluminescence is required (Finkenzeller, 2008; Chi and Chou, 2010; Zhang et al., 2014a; Yu et al., 2022).

Adachi's group, recently, has purported a novel triplet-harvesting mechanism named thermally activated delayed fluorescence (TADF) for highly proficient OLEDs as a workable alternative method with greater singlet yield (Endo et al., 2009; Mehes et al., 2012; Uoyama et al., 2012; Youn Lee et al., 2012; Li et al., 2020). For proficient TADF emitters, a narrower energy gap (ΔE_{ST}) amid the lowest singlet excited state (S_1) and lowest triplet excited state (T_1) is essential for reversible inter-system crossing (RISC) from the $T_1 \rightarrow S_1$ state (Berberan-Santos and Garcia, 1996; Wada et al., 2020). The ΔE_{ST} is associated with exchange energy (***j***) between the HOMOs and LUMOs in a molecule (Lu et al., 2015a). A tiny spatial overlap (***ρ***) amid HOMO-LUMO is believed to be an essential component (Lu et al., 2015b) for obtaining a low ΔE_{ST} value, and this is realized by joining the donor (**D**) and the acceptor (**A**) fragments in structures via steric hindrance, for instance, bulk, spirojunction, or homoconjugation (Kawasumi et al., 2015; Lu et al., 2016; Liu et al., 2020; Zhang et al., 2022).

Diphenylsulphone (**DPS**) unit is a versatile fragment with favorable features for TADF materials owing to a twist angle in the center and a high electron-accepting capacity (Huang et al., 2014; Tao et al., 2014; Bryden and Zysman-Colman, 2021). The sulfonyl group has an electron-withdrawing characteristic because of significant electronegativity of the oxygen atom in the group. It can also prevent compounds from undergoing π-conjugation because of its tetrahedral structure. High-performance TADF-OLEDs have been recognized by several sulfone-based compounds. As a result, in recent years, **DPS** has emerged as the most popular electron-accepting moiety for TADF emitters (Ye et al., 2013; Wu et al., 2014; Li et al., 2015; Liu et al., 2015). Several **DPS**-containing compounds with TADF properties have previously been described by Adachi's group (Zhang et al., 2012b; Ye et al., 2013; Wu et al., 2014; Li et al., 2015; Liu et al., 2015; Cui et al., 2020). Dimethylacridine-Diphenylsulphone (**DMAC-DPS**), among all the previously described **DPS**-based emitters, has been revealed to be a powerful blue TADF emitter with emission wavelength (λ_{em}) of 460 nm in toluene and ΔE_{ST} (CT) value of 0.02 eV (Zhang et al., 2014a; Luo et al., 2016). In order to adjust the emission color, our group has published a chain of derivatives using H/R substitution on the D and A units (R = CH_3 and CN) and "CH/N" substitution on the **D**-fragment (Wang et al., 2017a). It was discovered that modifying the **D** and **A** fragments with push-pull substituents is a useful technique for adjusting the λ_{em}, reducing the ΔE_{ST}, and enhancing the optical characteristics of designed molecules (Fan et al., 2016a; Lin et al., 2017a; Wang et al., 2017b; Yang et al., 2020; Jiao et al., 2021; Zhang et al., 2022). The "CH/N" as well as "H/CN" substitution on the acceptor unit, which results in bathochromically-shifted λ_{em} values and decreases ΔE_{ST} values, is a successful strategy, according to our analysis (Sun et al., 2008a; Sun et al., 2008b; Li et al., 2012).

In this contribution, we use the parent molecule **DMDHPN-DPS** (**1a**) as a starting point from our aforementioned report (Wang et al., 2017a). Then, by "CH/N" as well as "H/CN" substitution at meta and ortho sites of the **DPS** A-fragment, we were able to change the emission color to fashion blue TADF emitters. Figure 1 illustrates the structures of the parent molecule and all the symmetric substituted molecules. By computing ΔE_{ST} and λ_{em} values with the optimal Hartree-Fock percentage (OHF%) method in the exchange-correlation of the time-dependent density functional (TD-DFT) theory, we were able to analyse the TADF of these designed molecules.

2 Computational methodology

At first, the Gaussian-09 program was utilized to perform the ground state geometry optimization (S_0) for all of the derivatives employing B3LYP/6-31G(d) method. In addition, vibrational frequency analysis was accomplished to validate the local minima, and they turned up no imaginary frequencies (Irfan et al., 2014; Gao et al., 2017a; Gao et al., 2017b; Liu et al., 2022). Following that, the charge-transfer index (q), which is a measure of electron density re-distribution within a molecule, was determined from **D** to **A** using the HOMO and LUMO distribution. Subsequently, to examine the orbital composition using the Multiwfn tool, the optimal HF% (OHF%) was calculated using the relationship OHF = 42q. Based on S_0 geometry, the vertical absorption energies for singlet E_{VA} (S_1) as well as triplet E_{VA} (T_1) were computed using different functionals including M06-HF, M06-

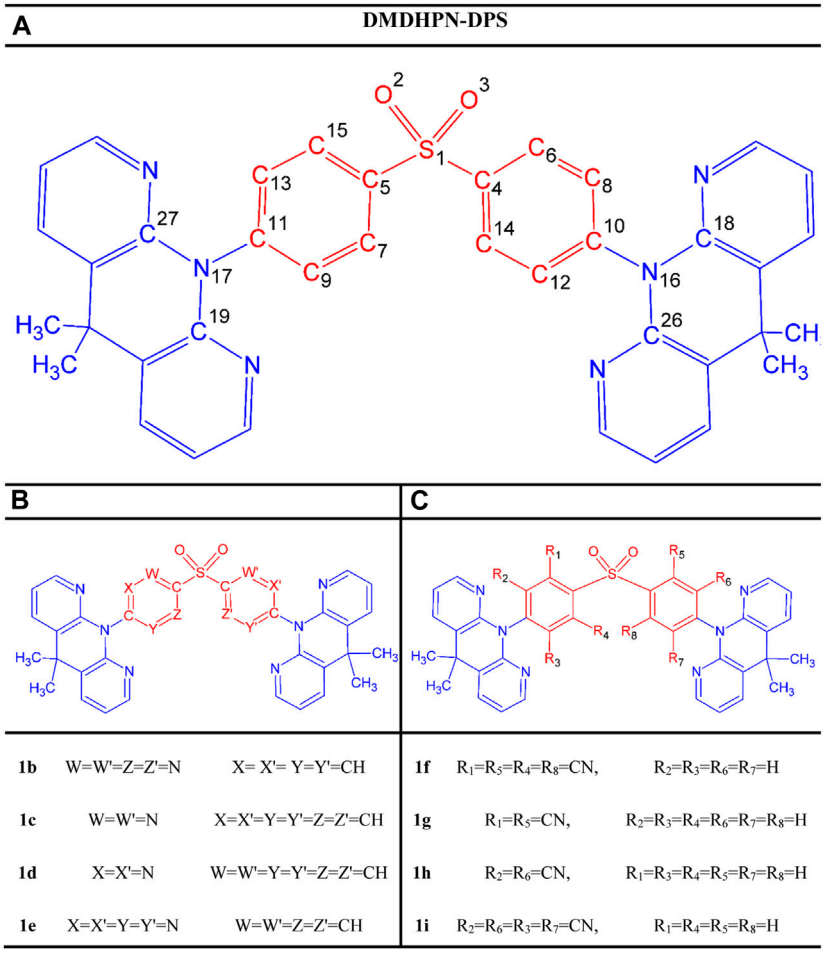

FIGURE 1
Scheme of the study showing the molecular structures of the parent molecule **(A)** and designed molecules **(B,C)** representing the CH/N and H/CN substituted derivatives, respectively.

2X, BMK, MPW1B95, PBE0, and B3LYP having different HF% of 100%, 54%, 42%, 31%, 25%, and 20%, respectively, with 6-31G(d) basis set. The HF percentage (HF%) of various functionals is given in Supplementary Figure S1. Afterward, the best-fit straight line of the double log plots of E_{VA} (S_1, T_1) against HF% was used to calculate the vertical excitation energy E_{VA} (S_1, OHF) as seen in Figure 2 and S1. Eventually, the ΔE_{ST} and zero-zero transition energies ($E_{0\text{-}0}$) were predicted using the following proven formulae of Adachi et al. (Huang et al., 2013; Zhang et al., 2014b; Tian et al., 2016; Cui et al., 2020).

$$E_{0-0}(1_{CT}) = E_{VA}(S_1, OHF) - \Delta E_V - \Delta E_{stokes} \quad (1)$$

$$E_{0-0}(3_{CT}) = E_{0-0}(1_{CT}) - E_{VA}(S_1, OHF) + \frac{E_{VA}(S_1, OHF)}{E_{VA}(S_1, B3LYP)} \times E_{VA}(T_1, B3LYP) \quad (2)$$

$$E_{0-0}(3_{LE}) = E_{VA}(T_1, B3LYP)/C - \Delta E_{stokes} \quad (3)$$

Here, ΔE_{stokes} (energy loss during Stokes-shift) is about 0.09 eV, and ΔE_V (difference in vibrational energy levels between the zero-zero transitions and the vertical transitions) is around 0.15 eV for the conjugated compounds. E_{VA} (T_1, B3LYP) depicts the vertical

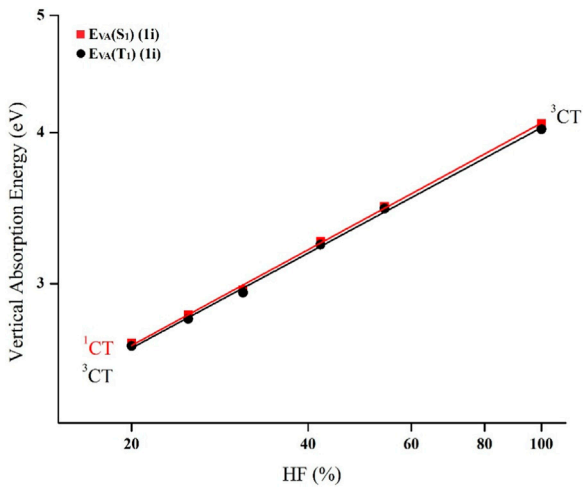

FIGURE 2
TD-DFT dependence of E_{VA} (S_1) as well as E_{VA} (T_1) on HF% in plotted on double log scale for the substituent **1i**.

TABLE 1 Computed E_{VA} (S_1), E_{VA} (T_1), CT amount (q), OHF%, $E_{0\text{-}0}$(^{1}CT), $E_{0\text{-}0}$(^{3}CT), and $E_{0\text{-}0}$ (^{3}LE) employing several functionals and 6-31G(d) basis set based on B3LYP/6-31G(d) optimized geometries of the designed substituents 1f–1i. (1a–1e are shown in Supplementary Table S6).

Parameter	Functional	1f	1g	1h	1i
E_{VA} (S_1) (eV)	B3LYP	2.8229	3.0381	3.0462	2.6772
	PBE1PBE	2.9791	3.2111	3.2030	2.8262
	MPWB95	3.1182	3.3666	3.3420	2.9645
	BMK	3.4277	3.7165	3.6559	3.2528
	M06-2X	3.6560	3.9666	3.8702	3.4756
	M06-HF	4.3066	4.7190	4.5220	4.0686
E_{VA} (T_1) (eV)	B3LYP	2.6443	2.9874	3.0235	2.6639
	PBE1PBE	2.6950	3.0449	3.0970	2.8052
	MPWB95	2.8800	3.2675	3.3060	2.9488
	BMK	3.1009	3.4712	3.5358	3.2319
	M06-2X	3.3253	3.7124	3.7775	3.4619
	M06-HF	3.8135	4.0671	4.1056	4.0260
CT amount (q)		0.8417	0.8828	0.8539	0.8295
OHF%		35	37	36	35
E_{VA} (S_1, OHF) (eV)		3.27	3.58	3.50	3.09
$E_{0\text{-}0}$ (^{1}CT) (eV)		3.03	3.34	3.26	2.85
$E_{0\text{-}0}$ (^{3}CT) (eV)		2.82	3.28	3.23	2.84
$E_{0\text{-}0}$ (^{3}LE) (eV)		2.77	3.06	3.07	2.90

excitation energy for the triplet (T_1) state calculated via B3LYP/6-31G(d) method. The C is the correction factor whose value for BMK, M06-2X, and, M06-HF functionals is about 1.10, 1.18, and 1.30, respectively. The S_1 state geometries were subsequently optimized using functionals with an HF% near the OHF (%). The MPW1B95 functional was selected for S_1 state optimization for all the studied derivatives as the OHF was determined to be closest to 31% as shown in Table 1. Then, using the TD-MPW1B95/6-31G(d) method with a polarizable continuum model (PCM) in the toluene medium, the absorption (λ_{ab}) and emission (λ_{em}) wavelengths were determined based on optimized S_0 and S_1 state geometries respectively. The Gaussian-09 software is used for all calculations (Fan et al., 2016b; Cai et al., 2016; Liu et al., 2020). Software such as Multiwfn, PyMOlyze, Origin, Gaussview, and Gausssum were used for postprocessing the findings.

3 Results and discussion

3.1 Optimized geometries at S_0 and S_1 states

Generally speaking, the photophysical characteristics of molecules with conjugated systems depend greatly on the dihedral angle and bond length. Stronger absorption, more effective emission, and improved fluorescence characteristics are frequently the results of optimal conjugation and planarity. Supplementary Table S1 shows the optimized geometrical parameters at S_0 and S_1 state of the parent and designed derivatives at B3LYP/6-31G(d) coupled with TD-MPW1B95/6-31G(d) level, employing DFT and TD-DFT, respectively. It is observed that the "CH/N" derivatives possess smaller C–N = bond lengths than the original C-C bond lengths at the pyrimidine/pyridine ring of the A-fragment because of the greater electronegativity of the nitrogen atom which draws the electron density towards itself and shortens the C–N = bond. In contrast, the C–C bond lengths in "H/CN" derivatives are longer than the prior C–C bond lengths because the –CN group will increase the electron-withdrawing strength of the A-moiety and elongates the C–C bond length inside the ring.

Bond lengths mostly alter on the substituent atom and nearby atom when compared to the original molecule **1a**. For instance, C_4–N_{14} and C_4–N_6 bond lengths of **1b**, where C_{14} and C_6 have been replaced by –N = atom, have decreased by 0.064 and 0.069 Å, respectively, in the S_0 state and 0.071 and 0.070 Å in the S_1 optimized state. Also, the lengths of the neighboring bonds C_{12}–N_{14} and N_6–C_8 have lessened by 0.054 Å and 0.051 Å, respectively, in the S_0 state and 0.072 Å in the S_1 state. Conversely, for **1i**, where –CN group has been used to replace the H-atom at C_8 and C_{12}, and the C_8–C_6, C_{10}–C_8, C_{12}–C_{10}, and C_{14}–C_{12} bond lengths have risen by 0.065, 0.011, 0.010 and, 0.066 Å in S_0 state and 0.076, 0.004, 0.005, and 0.076 Å in S_1 state, respectively. The bond length values for C_{12}–C_{14} and C_6–C_8 are decreased by 0.019 Å in S_0 to S_1 transition while increased by 0.003 Å for C_8–C_{10} and C_{10}–C_{12}. The geometrical parameters compared in the S_0 state and S_1 states for the parent and designed molecules showed a bond lengths alteration of up to 0.038 Å in C–C and C–N = bonds and up to 0.067 Å in C–S bonds. For the C–S bonds, the bond lengths alteration in the S_0 state and S_1 state are more pronounced. All of the proposed compounds have shorter C–S bonds in the S_1 (0.045–0.067 Å) than they do in the S_0. But their neighboring N–C and C–C bond lengths increase in the range of (0.002–0.023 Å) in S_1 than those in the S_0 state with only a few exceptions. Hence, it is obvious that the "CH/N" derivatives possess smaller C–N = bond lengths while "H/CN" derivatives possess larger C–C bond lengths. In both types of derivatives, "CH/N" and "H/CN", the conjugation is increased compared with parent molecule **1a**, hence there is a red-shift in wavelength.

We know that the greater the value of the torsional/dihedral angle (β) between D and A fragments, the smaller will be the HOMO-LUMO overlap and the lower will be the value of $\triangle E_{ST}$. It can be seen from Supplementary Table S1 that all the derivatives have large dihedral angle values (~85°–98°) between the D and A fragments in the S_0 state except **1b** (70.2°) due to the greater steric hindrance and **1f** (115.8°) due to the smaller steric hindrance. The larger β values for almost all the derivatives are optimistic for blocking the electrical interaction between D and A units (Zhang et al., 2014b; Lin et al., 2017b).

3.2 Frontier molecular orbitals

It is acknowledged that the frontier molecular orbitals (FMOs) offer crucial details on the nature of the TADF. The HOMO-LUMO electron density graphs at the S_0 state are displayed in Figure 3. Using the below relation in the Multiwfn program, the overlap between HOMO and LUMO (ρ) was calculated using.

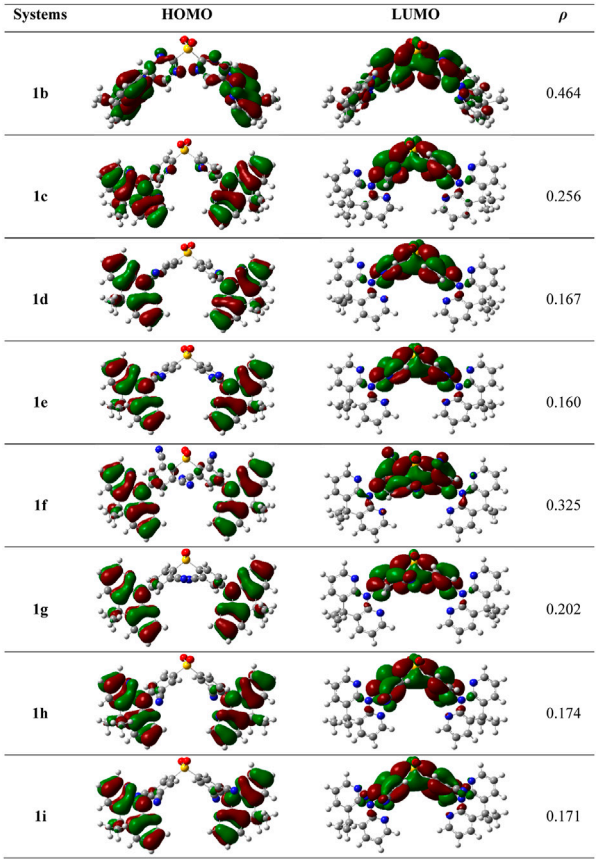

FIGURE 3
The electron density diagrams of HOMOs and LUMOs and the overlap between them in whole space for these studies compounds in S_0 geometry. The isosurface value for FMOs is 0.02.

$$\int |\varphi_i(\boldsymbol{r})||\varphi_j(\boldsymbol{r})|d\boldsymbol{r} \tag{4}$$

As is obvious from Figure 3, the HOMOs are particularly localized on the **DMDHPN** donor fragment while the LUMOs are largely distributed on the **DPS** acceptor moiety. Additionally, we found that the ρ values are ranging from 0.160 to 0.256, showing an ease of charge transfer between HOMO and LUMO, and a low electron exchange energy (***j***), which makes the ΔE_{ST} very modest except **1f** (0.325) and **1b** (0.464). Because the LUMO is mainly found on the A-unit of substituted derivatives, more substantial changes can be found in LUMO energy levels than HOMO energy levels, as seen in Figure 4. The energetic gaps ($\Delta E_{H\text{-}L}$) between HOMO and LUMO are in the range of 3.84–4.69 eV in the S_1 state and 3.40–4.45 eV in the S_0 state.

When –N = atom or –CN groups are added to A-fragments, the values of $\Delta E_{H\text{-}L}$ are lower than they would be for the parent molecule because the enhanced electron-accepting capacity of the **DPS** acceptors lowers the LUMO energy level, as shown in Supplementary Table S2. However, the LUMO energy levels are reduced more effectively by the –CN group than by the –N = atom, which reduces the $\Delta E_{H\text{-}L}$.

Additionally, the shift in $\Delta E_{H\text{–}L}$ values is more apparent as the greater number of –CN groups or –N = atoms there are. Given that

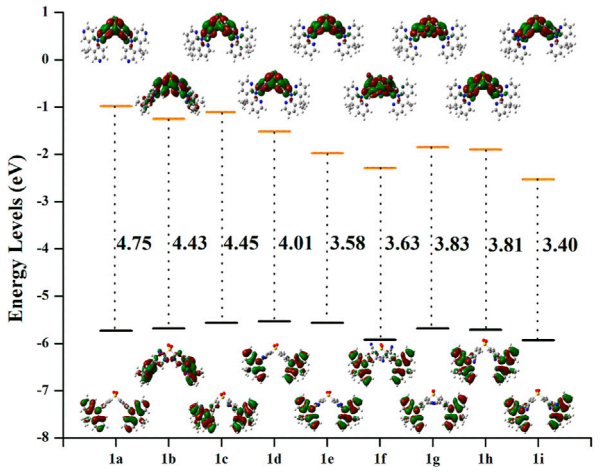

FIGURE 4
The electron density diagrams and HOMO-LUMO energetic gap of the studies molecules in the S_0 state. The isosurface value for FMOs is 0.02.

the λ_{ab} and λ_{em} values are connected to the $\Delta E_{H\text{–}L}$ values, (Li et al., 2012), the import of –CN groups or of –N = atoms to the A-fragments may alter the absorption and emission spectra, as illustrated in Supplementary Tables S4, S5. As a result, it is expected that the newly created derivatives would exhibit red-shifted λ_{em} when compared to the parent molecule **1a**.

3.3 Singlet-triplet energy gap

Using the Multiwfn program, the $E_{0\text{-}0}$ (S_1), $E_{0\text{-}0}$ (^{3}CT), as well as $E_{0\text{-}0}$ (^{3}LE) are attained based on the computed CT amount (q) (Table 1). At first, double log plots of E_{VA} (S_1, T_1) versus HF% for the compounds under investigation were plotted (Figure 2). Then the $E_{0\text{-}0}$ (S_1), $E_{0\text{-}0}$ (^{3}CT), as well as $E_{0\text{-}0}$ (^{3}LE) of these designed derivatives were computed using Eqs 1–3 as shown in Table 3. The calculated findings for the substituted molecules show that the addition of –CN groups or of –N = atoms on the A-moiety improves its capacity to pull electrons, which eventually leads to a decrease in the ΔE_{ST} value. Additionally, it is clear that as there are more –CN groups or of –N = atoms, the ΔE_{ST} values decrease, particularly at meta-position. It is also obvious that the "CH/N" derivatives have lower ΔE_{ST} values than the original molecule but are larger than the "H/CN" derivatives. When the lowest T_1 state is taken into account, the computed $E_{0\text{-}0}$ (^{3}CT), as well as $E_{0\text{-}0}$ (^{3}LE), appear to have the lowest energy levels. The ^{1}CT–^{3}CT splitting is denoted by ΔE_{ST} (CT), while the energy difference amid the lowest T_1 and the S_1 state is denoted by $\Delta E_{S1\text{-}T1}$ (Huang et al., 2013). All the newly designed molecules are symmetric substitution derivatives and have lower ΔE_{ST} values as compared with a parent molecule. According to Table 2, for **1i,** the T_1 state is ^{3}CT in nature, which is ideal for an effectual RISC, whereas, for others, T_1 states are ^{3}LE in nature. The calculated ΔE_{ST} (CT) value using the OHF method for **1i** is 0.01 eV resulting from the small ρ value. The **1i** has the smallest ΔE_{ST} value compared with all the other substituted derivatives because 1) it is a "H/CN" substituted derivative which is more effective than "CH/N"

TABLE 2 Computed ΔE_{ST} (CT) and $\Delta E_{S1\text{-}T1}$ for the studies molecules.

Molecules	$E_{0\text{-}0}$ (^{1}CT) (eV)	$E_{0\text{-}0}$ (^{3}CT) (eV)	$E_{0\text{-}0}$ (^{3}LE) (eV)	ΔE_{ST} (CT) (eV)	$\Delta E_{S1\text{-}T1}$ (eV)
1a	4.04	3.46	3.07 (T_1)	0.58	0.97
1b	3.44	3.21	3.05 (T_1)	0.23	0.39
1c	3.75	3.46	3.03 (T_1)	0.29	0.72
1d	3.54	3.52	3.10 (T_1)	0.02	0.44
1e	3.14	3.13	3.04 (T_1)	0.01	0.10
1f	3.03	2.82	2.77 (T_1)	0.21	0.26
1g	3.34	3.27	3.07 (T_1)	0.07	0.27
1h	3.26	3.23	3.07 (T_1)	0.03	0.19
1i	2.85	2.84 (T_1)	2.90	0.01	−0.05

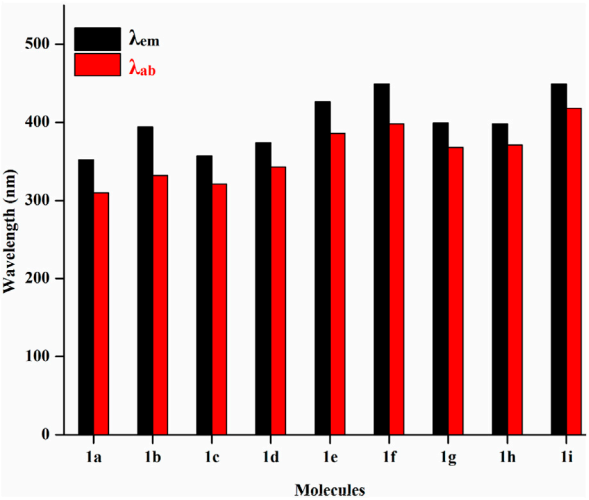

FIGURE 5
Absorption and emission spectrum of the studied molecules.

substituted derivatives 2) two H-atoms have been replaced with two CN-groups which will further enhance the electron-withdrawing strength of the A-fragment 3) it is meta-substituted and is at a greater distance from sulphonyl group. Even though some other designed molecules, including the selected violet-blue to blue derivates like **1b**, **1f**, **1g**, and **1h**, possess a lower ^{3}LE state, the effective TADF is made feasible via reversible internal conversion from ^{3}LE to ^{3}CT state followed by a subsequent RISC from ^{3}CT to ^{1}CT state. So, by enhancing the electron-withdrawing capacity of A, it is beneficial to raise the ^{3}LE state and lower the ΔE_{ST} (Hussain et al., 2019; Hassan et al., 2022; Hussain et al., 2023).

3.4 Photophysical properties

Figure 5 displays the emission and absorption spectra of the parent molecule and all derivatives. Table 3 lists the estimated emission and absorption wavelengths (λ_{em} and λ_{ab}) in the toluene medium at the TD-MPW1B95/6-31G(d) theory level. All the investigation molecules have λ_{em} and λ_{ab} values corresponding to the values of $\Delta E_{H\text{-}L}$. The designed derivatives show that the λ_{em} and λ_{ab} values range from 357 to 449 nm and 321–418 nm, respectively. The λ_{em} bands instigate from $S_1 \rightarrow S_0$ transitions which is mainly the transference of the electrons from LUMO → HOMO, and the electronic shifts are $\pi^* \rightarrow \pi$ type. The addition of –CN group or –N = atom to **DPS** acceptor moiety has resulted in the bathochromically-shifted values for λ_{em} and λ_{ab}. Furthermore, by increasing the numbers of –CN groups or –N = atoms, the λ_{em}, and λ_{ab} values display a more significant red-shift. Particularly, the derivatives **1f** and **1i,** display a more noticeable red-shift in λ_{em} of about 97 nm each. Additionally, the meta-positioned derivatives show more red-shift in λ_{em} and λ_{ab} values than ortho-positions with the same number of –CN groups or of –N = atoms. Actually, at meta-position, the –CN group or –N = atom is at a larger distance from the sulphonyl group and experiences less steric hindrance compared to the ortho position which experiences more steric repulsion. It will increase the stability and charge transfer characters of the substituted derivatives which results in lowering the ΔE_{ST} and increasing the λ_{em} value. It is evident from the calculated results that the three molecules named **1b**, **1g**, and **1h** are showing violet-blue emission (394, 399, and 398 nm) and two of them named **1f** and **1i** are showing blue emission of 449 nm with reasonable emission intensity peak demonstrating that the studied compounds are effective violet-blue to blue TADF materials. We can see that both **1f** and **1i** have the same value of emission wavelength (λ_{em}) of 449 nm lying in the pure blue region but **1i** is regarded as a comparatively better TADF candidate as it has a lower ΔE_{ST} 0.01 eV value as compared to **1f** (0.26 eV). The constructed molecules demonstrated that the sequence of λ_{ab}, as well as λ_{em}, is coherent with the propensity of the electron-withdrawing strength of A-fragment.

The energy (or wavelength) differential between a molecule's absorption (λ_{ab}) and emission (λ_{em}) maxima is called as the Stokes-shift ($\Delta\upsilon$). It represents the energy loss occurring during the $S_1 \rightarrow S_0$ transition. In general, a smaller Stokes-shift is advantageous since it decreases the spectral overlap between excitation and emission signals. Since self-absorption is reduced by a narrow Stokes-shift, more of the absorbed energy is transformed into light output, enhancing OLEDs' total energy

TABLE 3 Calculated λ_{ab} and λ_{em} values in toluene for the studied molecules employing TD-MPW1B95/6-31G(d) method based on S_0 and S_1 state optimized geometries, respectively, along with Stoke Shift ($\Delta\upsilon$) values.

Molecule	Wavelength λ_{ab} (nm)	Oscillator strength (*f*)	Wavelength λ_{em} (nm)	Oscillator strength (*f*)	Stoke shift ($\Delta\upsilon$) ($\Delta\upsilon = \lambda_{em}-\lambda_{ab}$)
1a	310	0.0015	352	0.1385	42
1b	332	0.0723	394	0.1682	62
1c	321	0.0069	357	0.2464	36
1d	343	0.0010	374	0.0005	31
1e	386	0.0003	426	0.0001	40
1f	398	0.1921	449	0.0081	51
1g	368	0.0182	399	0.0473	31
1h	371	0.0047	398	0.0159	27
1i	418	0.0005	449	0.0165	31

efficiency. Every constructed molecule, except **1b** and **1f**, exhibits a smaller stokes-shift than the original molecule as shown in Table 3. It is also obvious that the "H/CN" substituents exhibit a relatively smaller value compared with "CH/N" derivatives hence more effective in reducing the energy loss during the $S_1 \rightarrow S_0$ transition.

4 Conclusion

In conclusion, we have projected the photophysical as well as electronic characteristics for a variety of freshly created substituents to improve the efficacies for blue TADF emitters based on the parent system **DMDHPN-DPS**. The HOMOs are primarily concentrated on the **DMDHPN**-donor moiety, whereas the LUMOs are located at the **DPS**-acceptor unit. The λ_{em} of all the designed derivatives ranges from 357 to 449 nm. The import of –CN groups or of –N = atoms on **DPS** moiety lowers the transition energy from LUMO to HOMO, causing a red-shift in λ_{em}. Additionally, the red-shift in λ_{em} values becomes more significant by increasing the quantity of –CN groups or of –N = atoms. The derivatives **1f** and **1i** display a more evident red-shift of 97 nm. Additionally, meta-position substituents exhibit greater red-shifted λ_{em} values than ortho-position substituents with the same number of –CN groups or of –N = atoms. Actually, at meta-position, the –CN group or –N = atom is at a larger distance from the sulphonyl group and experiences less steric hindrance compared to the ortho position which experiences more steric repulsion. It will increase the stability and charge transfer characters of the substituted derivatives which result in lowering the ΔE_{ST} and increasing the λ_{em} value. The small ρ values for the designed molecules due to the greater β values of 85°–98° contribute to the realization of the charge transfer state and small ΔE_{ST}. The estimated findings showed that, out of all the analyzed molecules, three violet-blue emitters (394–399 nm) and two blue emitters (449 nm) with reasonable emission intensity and smaller ΔE_{ST} are favorable to be effective violet-blue to blue TADF emitters with **1i** being the best TADF candidate as it has smallest ΔE_{ST} values of 0.01 eV. We believe that in the future, understanding and building effective violet-blue to blue TADF-based OLEDs will be made easier with the aid of our theoretical designs.

Data availability statement

The original contributions presented in the study are included in the article/Supplementary Material, further inquiries can be directed to the corresponding authors.

Author contributions

AH: Conceptualization, Data curation, Formal Analysis, Investigation, Methodology, Project administration, Software, Supervision, Validation, Visualization, Writing–original draft, Writing–review and editing. AI: Formal Analysis, Funding acquisition, Project administration, Resources, Supervision, Validation, Visualization, Writing–original draft. FK: Conceptualization, Formal

Analysis, Investigation, Methodology, Supervision, Writing–original draft. MAf: Investigation, Methodology, Writing–review and editing. AC: Investigation, Methodology, Software, Writing–review and editing. MH: Formal analysis, Investigation, Methodology, Writing–review and editing. MAl: Formal Analysis, Investigation, Writing–review and editing.

Funding

The authors declare financial support was received for the research, authorship, and/or publication of this article.

Acknowledgments

AI extends his appreciation to the Deanship of Scientific Research at King Khalid University for funding this work through Large Groups Project under grant number (RGP2/276/44). AC is thankful to the Deanship of Scientific Research at the University of Bisha, for supporting this work through the Fast-Track Research Support Program. We are also acknowledging the school of Chemistry, University of the Punjab, Lahore, Pakistan for providing research facilities.

Conflict of interest

The authors declare that the research was conducted in the absence of any commercial or financial relationships that could be construed as a potential conflict of interest.

The reviewer MQ declared a past co-authorship with the author AI to the handling editor.

Publisher's note

Supplementary material

The Supplementary Material for this article can be found online at: https://www.frontiersin.org/articles/10.3389/fchem.2023.1279355/full#supplementary-material

References

Adachi, C., Baldo, M. A., Thompson, M. E., and Forrest, S. R. (2001). Nearly 100% internal phosphorescence efficiency in an organic light-emitting device. *J. Appl. Phys.* 90 (10), 5048–5051. doi:10.1063/1.1409582

Berberan-Santos, M. N., and Garcia, J. M. M. (1996). Unusually strong delayed fluorescence of C70. *J. Am. Chem. Soc.* 118 (39), 9391–9394. doi:10.1021/ja961782s

Bryden, M. A., and Zysman-Colman, E. (2021). Organic thermally activated delayed fluorescence (TADF) compounds used in photocatalysis. *Chem. Soc. Rev.* 50 (13), 7587–7680. doi:10.1039/d1cs00198a

Cai, X., Li, X., Xie, G., He, Z., Gao, K., Liu, K., et al. (2016). Rate-limited effect of reverse intersystem crossing process: the key for tuning thermally activated delayed fluorescence lifetime and efficiency roll-off of organic light emitting diodes. *Chem. Sci.* 7 (7), 4264–4275. doi:10.1039/c6sc00542j

Chan, C.-Y., Cui, L.-S., Kim, J. U., Nakanotani, H., and Adachi, C. (2018). Rational molecular design for deep-blue thermally activated delayed fluorescence emitters. *Adv. Funct. Mater.* 28 (11), 1706023. doi:10.1002/adfm.201706023

Chi, Y., and Chou, P. T. (2010). Transition-metal phosphors with cyclometalating ligands: fundamentals and applications. *Chem. Soc. Rev.* 39 (2), 638–655. doi:10.1039/b916237b

Cui, L.-S., Gillett, A. J., Zhang, S.-F., Ye, H., Liu, Y., Chen, X.-K., et al. (2020). Fast spin-flip enables efficient and stable organic electroluminescence from charge-transfer states. *Nat. Photonics* 14 (10), 636–642. doi:10.1038/s41566-020-0668-z

Deaton, J. C., Switalski, S. C., Kondakov, D. Y., Young, R. H., Pawlik, T. D., Giesen, D. J., et al. (2010). E-type delayed fluorescence of a phosphine-supported Cu2(μ-NAr2) 2 diamond core: harvesting singlet and triplet excitons in OLEDs. *J. Am. Chem. Soc.* 132 (27), 9499–9508. doi:10.1021/ja1004575

Endo, A., Ogasawara, M., Takahashi, A., Yokoyama, D., Kato, Y., and Adachi, C. (2009). Thermally activated delayed fluorescence from Sn(4+)-porphyrin complexes and their application to organic light emitting diodes--a novel mechanism for electroluminescence. *Adv. Mater.* 21 (47), 4802–4806. doi:10.1002/adma.200900983

Fan, J., Lin, L., and Wang, C. (2016a). Modulating excited state properties of thermally activated delayed fluorescence molecules by tuning the connecting pattern. *Theor. Chem. Accounts* 135 (7), 169. doi:10.1007/s00214-016-1928-3

Fan, J.-z., Lin, L.-l., and Wang, C.-k. (2016b). Decreasing the singlet–triplet gap for thermally activated delayed fluorescence molecules by structural modification on the donor fragment: first-principles study. *Chem. Phys. Lett.* 652, 16–21. doi:10.1016/j.cplett.2016.04.027

Finkenzeller, H. Y. A. W. J. (2008). *Highly efficient OLEDs with phosphorescent materials*. Weinheim: Wiley VCH: KGaA, 1–97.

Gao, Y., Geng, Y., Wu, Y., Zhang, M., and Su, Z.-M. (2017a). Investigation on the effect of connected bridge on thermally activated delayed fluorescence property for DCBPy emitter. *Dyes Pigments* 145, 277–284. doi:10.1016/j.dyepig.2017.04.001

Gao, Y., Su, T., Zhao, L., Geng, Y., Wu, Y., Zhang, M., et al. (2017b). How does a little difference in structure determine whether molecules have thermally activated delayed fluorescence characteristic or not? *Org. Electron.* 50, 70–76. doi:10.1016/j.orgel.2017.07.024

Hassan, M., Baig, M. M., Shah, K. H., Hussain, A., Hassan, S. A., and Ali, A. (2022). MOF-based bimetallic diselenide nanospheres as a bifunctional efficient electrocatalysts for overall water splitting. *J. Phys. Chem. Solids* 167, 110780. doi:10.1016/j.jpcs.2022.110780

Huang, B., Qi, Q., Jiang, W., Tang, J., Liu, Y., Fan, W., et al. (2014). Thermally activated delayed fluorescence materials based on 3,6-di-tert-butyl-9-((phenylsulfonyl)phenyl)-9H-carbazoles. *Dyes Pigments* 111, 135–144. doi:10.1016/j.dyepig.2014.06.008

Huang, S., Zhang, Q., Shiota, Y., Nakagawa, T., Kuwabara, K., Yoshizawa, K., et al. (2013). Computational prediction for singlet- and triplet-transition energies of charge-transfer compounds. *J. Chem. Theory Comput.* 9 (9), 3872–3877. doi:10.1021/ct400415r

Hussain, A., Kanwal, F., Irfan, A., Hassan, M., and Zhang, J. (2023). Exploring the influence of engineering the linker between the donor and acceptor fragments on thermally activated delayed fluorescence characteristics. *ACS Omega* 8, 15638–15649. doi:10.1021/acsomega.3c01098

Hussain, A., Yuan, H., Li, W., and Zhang, J. (2019). Theoretical investigations of the realization of sky-blue to blue TADF materials via CH/N and H/CN substitution at the diphenylsulphone acceptor. *J. Saudi Chem. Soc.* 7 (22), 6685–6691. doi:10.1039/c9tc01449g

Irfan, A., Aftab, H., and Al-Sehemi, A. G. (2014). Push–pull effect on the geometries, electronic and optical properties of thiophene based dye-sensitized solar cell materials. *J. Saudi Chem. Soc.* 18 (6), 914–919. doi:10.1016/j.jscs.2011.11.013

Jiao, Y., Đorđević, L., Mao, H., Young, R. M., Jaynes, T., Chen, H., et al. (2021). A donor–acceptor [2] catenane for visible light photocatalysis. *J. Am. Chem. Soc.* 143 (21), 8000–8010. doi:10.1021/jacs.1c01493

Kawasumi, K., Wu, T., Zhu, T., Chae, H. S., Van Voorhis, T., Baldo, M. A., et al. (2015). Thermally activated delayed fluorescence materials based on homoconjugation effect of donor-acceptor triptycenes. *J. Am. Chem. Soc.* 137 (37), 11908–11911. doi:10.1021/jacs.5b07932

Li, W., Li, Z., Si, C., Wong, M. Y., Jinnai, K., Gupta, A. K., et al. (2020). Organic long-persistent luminescence from a thermally activated delayed fluorescence compound. *Adv. Mater.* 32 (45), 2003911. doi:10.1002/adma.202003911

Li, Y., Wang, Z., Li, X., Xie, G., Chen, D., Wang, Y.-F., et al. (2015). Highly efficient spiro[fluorene-9,9′-thioxanthene] core derived blue emitters and fluorescent/phosphorescent hybrid white organic light-emitting diodes. *Chem. Mater.* 27 (3), 1100–1109. doi:10.1021/cm504441v

Li, Y., Zou, L.-Y., Ren, A.-M., and Feng, J.-K. (2012). Theoretical study on the electronic structures and photophysical properties of a series of dithienylbenzothiazole derivatives. *Comput. Theor. Chem.* 981, 14–24. doi:10.1016/j.comptc.2011.11.021

Lin, L., Fan, J., and Wang, C.-K. (2017b). Theoretical perspective for internal quantum efficiency of thermally activated delayed fluorescence emitter in solid phase: a QM/MM study. *Org. Electron.* 51, 349–356. doi:10.1016/j.orgel.2017.09.021

Lin, L., Wang, Z., Fan, J., and Wang, C. (2017a). Theoretical insights on the electroluminescent mechanism of thermally activated delayed fluorescence emitters. *Org. Electron.* 41, 17–25. doi:10.1016/j.orgel.2016.11.035

Liu, M., Seino, Y., Chen, D., Inomata, S., Su, S. J., Sasabe, H., et al. (2015). Blue thermally activated delayed fluorescence materials based on bis(phenylsulfonyl)benzene derivatives. *Chem. Commun.* 51 (91), 16353–16356. doi:10.1039/c5cc05435d

Liu, T., Deng, C., Duan, K., Tsuboi, T., Niu, S., Wang, D., et al. (2022). Zero–zero energy-dominated degradation in blue organic light-emitting diodes employing thermally activated delayed fluorescence. *ACS Appl. Material Interfaces* 14 (19), 22332–22340. doi:10.1021/acsami.2c02623

Liu, Y., Wei, X., Li, Z., Liu, J., Wang, R., Hu, X., et al. (2018). Highly efficient, solution-processed organic light-emitting diodes based on thermally activated delayed-fluorescence emitter with a mixed polymer interlayer. *ACS Appl. Energy Mater.* 1 (2), 543–551. doi:10.1021/acsaem.7b00131

Liu, Y., Yuan, Y., Tian, X., and Sun, J. (2020). Theoretical investigation on reverse intersystem crossing from upper triplet to lowest singlet: a "hot exciton" path for blue fluorescent OLEDs. *Int. J. Quantum Chem.* 120 (23), e26399. doi:10.1002/qua.26399

Lu, J., Zheng, Y., and Zhang, J. (2015a). Tuning the color of thermally activated delayed fluorescent properties for spiro-acridine derivatives by structural modification of the acceptor fragment: a DFT study. *RSC Adv.* 5 (24), 18588–18592. doi:10.1039/c4ra15155k

Lu, J., Zheng, Y., and Zhang, J. (2015b). Rational design of phenoxazine-based donor-acceptor-donor thermally activated delayed fluorescent molecules with high performance. *Phys. Chem. Chem. Phys.* 17 (30), 20014–20020. doi:10.1039/c5cp02810h

Lu, J., Zheng, Y., and Zhang, J. (2016). Computational design of benzo [1,2-b:4,5-b′] dithiophene based thermally activated delayed fluorescent materials. *Dyes Pigments* 127, 189–196. doi:10.1016/j.dyepig.2015.12.030

Luo, J., Gong, S., Gu, Y., Chen, T., Li, Y., Zhong, C., et al. (2016). Multi-carbazole encapsulation as a simple strategy for the construction of solution-processed, non-doped thermally activated delayed fluorescence emitters. *J. Mater. Chem. C* 4 (13), 2442–2446. doi:10.1039/c6tc00418k

Mehes, G., Nomura, H., Zhang, Q., Nakagawa, T., and Adachi, C. (2012). Enhanced electroluminescence efficiency in a spiro-acridine derivative through thermally activated delayed fluorescence. *Angew. Chem. Int. Ed. Engl.* 51 (45), 11311–11315. doi:10.1002/anie.201206289

Shuai, Z., Beljonne, D., Silbey, R. J., and Brédas, J. L. (2000). Singlet and triplet exciton formation rates in conjugated polymer light-emitting diodes. *Phys. Rev. Lett.* 84 (1), 131–134. doi:10.1103/physrevlett.84.131

Sun, H., Zhong, C., and Bredas, J. L. (2015). Reliable prediction with tuned range-separated functionals of the singlet-triplet gap in organic emitters for thermally activated delayed fluorescence. *J. Chem. Theory Comput.* 11 (8), 3851–3858. doi:10.1021/acs.jctc.5b00431

Sun, M., Niu, B., and Zhang, J. (2008a). Computational study on optical and electronic properties of the "CH"/N substituted emitting materials based on spirosilabifluorene derivatives. *J. Mol. Struct. THEOCHEM* 862 (1-3), 85–91. doi:10.1016/j.theochem.2008.04.038

Sun, M., Niu, B., and Zhang, J. (2008b). Theoretical design of blue emitting materials based on symmetric and asymmetric spirosilabifluorene derivatives. *Theor. Chem. Accounts* 119 (5-6), 489–500. doi:10.1007/s00214-008-0410-2

Tang, C. W., and VanSlyke, S. A. (1987). Organic electroluminescent diodes. *Appl. Phys. Lett.* 51 (12), 913–915. doi:10.1063/1.98799

Tao, Y., Yuan, K., Chen, T., Xu, P., Li, H., Chen, R., et al. (2014). Thermally activated delayed fluorescence materials towards the breakthrough of organoelectronics. *Adv. Mater.* 26 (47), 7931–7958. doi:10.1002/adma.201402532

Tian, X., Sun, H., Zhang, Q., and Adachi, C. (2016). Theoretical predication for transition energies of thermally activated delayed fluorescence molecules. *Chin. Chem. Lett.* 27 (8), 1445–1452. doi:10.1016/j.cclet.2016.07.017

Uoyama, H., Goushi, K., Shizu, K., Nomura, H., and Adachi, C. (2012). Highly efficient organic light-emitting diodes from delayed fluorescence. *Nature* 492 (7428), 234–238. doi:10.1038/nature11687

Wada, Y., Nakagawa, H., Matsumoto, S., Wakisaka, Y., and Kaji, H. (2020). Organic light emitters exhibiting very fast reverse intersystem crossing. *Nat. Photonics* 14 (10), 643–649. doi:10.1038/s41566-020-0667-0

Wang, J., Lu, J., and Zhang, J. (2017a). Tuning the electronic and optical properties of diphenylsulphone based thermally activated delayed fluorescent materials via structural modification: a theoretical study. *Dyes Pigments* 143, 42–47. doi:10.1016/j.dyepig.2017.03.064

Wang, L., Li, T., Feng, P., and Song, Y. (2017b). Theoretical tuning of the singlet-triplet energy gap to achieve efficient long-wavelength thermally activated delayed fluorescence emitters: the impact of substituents. *Phys. Chem. Chem. Phys.* 19 (32), 21639–21647. doi:10.1039/c7cp02615c

Wu, S., Aonuma, M., Zhang, Q., Huang, S., Nakagawa, T., Kuwabara, K., et al. (2014). High-efficiency deep-blue organic light-emitting diodes based on a thermally activated delayed fluorescence emitter. *J. Mater. Chem. C* 2 (3), 421–424. doi:10.1039/c3tc31936a

Xu, Y., Wang, Q., Cai, X., Li, C., and Wang, Y. (2021). Highly efficient electroluminescence from narrowband green circularly polarized multiple resonance thermally activated delayed fluorescence enantiomers. *Adv. Mater.* 33 (21), 2100652. doi:10.1002/adma.202100652

Yang, S.-Y., Wang, Y.-K., Peng, C.-C., Wu, Z.-G., Yuan, S., Yu, Y.-J., et al. (2020). Circularly polarized thermally activated delayed fluorescence emitters in through-space charge transfer on asymmetric spiro skeletons. *J. Am. Chem. Soc.* 142 (41), 17756–17765. doi:10.1021/jacs.0c08980

Ye, J., Chen, Z., Fung, M.-K., Zheng, C., Ou, X., Zhang, X., et al. (2013). Carbazole/sulfone hybrid D-π-A-structured bipolar fluorophores for high-efficiency blue-violet electroluminescence. *Chem. Mater.* 25 (13), 2630–2637. doi:10.1021/cm400945h

Youn Lee, S., Yasuda, T., Nomura, H., and Adachi, C. (2012). High-efficiency organic light-emitting diodes utilizing thermally activated delayed fluorescence from triazine-based donor–acceptor hybrid molecules. *Appl. Phys. Lett.* 101 (9), 093306. doi:10.1063/1.4749285

Yu, R., Song, Y., Zhang, K., Pang, X., Tian, M., and He, L. (2022). Intrinsically ionic, thermally activated delayed fluorescent materials for efficient, bright, and stable light-emitting electrochemical cells. *Adv. Funct. Mater.* 32 (13), 2110623. doi:10.1002/adfm.202110623

Zhang, Q., Komino, T., Huang, S., Matsunami, S., Goushi, K., and Adachi, C. (2012a). Triplet exciton confinement in green organic light-emitting diodes containing luminescent charge-transfer Cu(I) complexes. *Adv. Funct. Mater.* 22 (11), 2327–2336. doi:10.1002/adfm.201101907

Zhang, Q., Kuwabara, H., Potscavage, W. J., Jr., Huang, S., Hatae, Y., Shibata, T., et al. (2014b). Anthraquinone-based intramolecular charge-transfer compounds: computational molecular design, thermally activated delayed fluorescence, and highly efficient red electroluminescence. *J. Am. Chem. Soc.* 136 (52), 18070–18081. doi:10.1021/ja510144h

Zhang, Q., Li, B., Huang, S., Nomura, H., Tanaka, H., and Adachi, C. (2014a). Efficient blue organic light-emitting diodes employing thermally activated delayed fluorescence. *Nat. Photonics* 8 (4), 326–332. doi:10.1038/nphoton.2014.12

Zhang, Q., Li, J., Shizu, K., Huang, S., Hirata, S., Miyazaki, H., et al. (2012b). Design of efficient thermally activated delayed fluorescence materials for pure blue organic light emitting diodes. *J. Am. Chem. Soc.* 134 (36), 14706–14709. doi:10.1021/ja306538w

Zhang, Y. P., Mao, M. X., Song, S. Q., Wang, Y., Zheng, Y. X., Zuo, J. L., et al. (2022). Circularly polarized white organic light-emitting diodes based on spiro-type thermally activated delayed fluorescence materials. *Angew. Chem.* 61, e202200290. doi:10.1002/anie.202200290